

Distinct global warming rates tied to multiple ocean surface temperature changes

Shuai-Lei Yao^{1,2}, Jing-Jia Luo^{3*}, Gang Huang^{1,2,4*} and Pengfei Wang^{1,5}

The globally averaged surface temperature has shown distinct multi-decadal fluctuations since 1900^{1–4}, characterized by two weak slowdowns in the mid-twentieth century and early twenty-first century and two strong accelerations in the early and late twentieth century. While the recent global warming (GW) hiatus has been particularly ascribed to the eastern Pacific cooling^{5,6}, causes of the cooling in the mid-twentieth century and distinct intensity differences between the slowdowns and accelerations remain unclear^{7,8}. Here, our model experiments with multiple ocean sea surface temperature (SST) forcing reveal that, although the Pacific SSTs play essential roles in the GW rates, SST changes in other basins also exert vital influences. The mid-twentieth-century cooling results from the SST cooling in the tropical Pacific and Atlantic, which is partly offset by the Southern Ocean warming. During the recent hiatus, the tropical Pacific-induced strong cooling is largely compensated by warming effects of other oceans. In contrast, during the acceleration periods, ubiquitous SST warming across all the oceans acts jointly to exaggerate the GW. Multi-model simulations with separated radiative forcing suggest diverse causes of the SST changes in multiple oceans during the GW acceleration and slowdown periods. Our results highlight the importance of multiple oceans on the multi-decadal GW rates.

The Paris Climate Conference in December 2015 has agreed to pursue efforts to limit the global warming (GW) to no more than 1.5 °C above pre-industrial levels by 2100 (ref. 9). The observed annual-mean globally averaged surface temperature (GST) has already risen about 0.89 °C (0.69–1.08 °C, 90% confidence interval)¹⁰ during the period 1900–2012 (Fig. 1 and Supplementary Table 1), leaving room for just another 0.5–0.6 °C warming relative to today for the rest of the twenty-first century. While the early twenty-first-century GW hiatus indicates that the relentlessly increasing greenhouse gases (GHGs) may not always boost the GST warming simultaneously⁶, it is yet unclear whether the recent hiatus has surely ended and how strongly GW will resume in the next decades. In addition, it is found that the GW rate since 1900 has experienced a pronounced multi-decadal fluctuation, characterized by two accelerations in the early and late twentieth century and two slowdowns during the mid-twentieth century and the early twenty-first century^{1,2} (Fig. 1). Correspondingly, the globally averaged land surface air temperature shows similar multi-decadal modulations. The distinctive multi-decadal fluctuation undoubtedly affects the estimation of centennial mean GW rate^{11,12}. Improved understanding of these GW accelerations and slowdowns could help provide a better estimate of the future GW rate for the Paris Climate Agreement.

The estimated rates of the multi-decadal GW accelerations and slowdowns are subject to the time interval selection¹³, which is often based on an arbitrary decision¹⁴. Here, the GW acceleration and slowdown periods are objectively determined according to three thresholds: a maximum magnitude of statistically significant trends in observed GST, relatively low uncertainty among different observations (represented by error bars in Supplementary Fig. 1), and a high percentage of global areas where the merged land air temperature and ocean surface temperature has a statistically significant trend (Supplementary Fig. 1 and Methods). Our approach identifies two periods with maximum accelerations of the GW during 1908–1945 and 1975–1998 and two periods with maximum slowdowns during 1940–1976 and 2001–2012 (Fig. 1).

It is found that observed GST trends during the two acceleration periods are statistically significant across four different observational data sets, whereas those during the two slowdown periods are less significant (Supplementary Table 1), especially for the early twenty-first-century slowdown. The latest slowdown does not show a consistently negative GW rate among the different observations and is statistically insignificant (Supplementary Table 1), probably owing to a relatively short period for the trend estimation. Despite this, the recent GW slowdown has received tremendous attention and has been examined extensively^{5,6,8}. The magnitudes of the GW rates during the two slowdown periods are considerably smaller than those during the two acceleration periods. This difference has been explained as being due to the naturally occurring decadal/multi-decadal climate variability halting the steady GW rate attributed to the continuously increasing GHGs emissions¹⁵. For instance, the recent slowdown has been tied to the equatorial Pacific sea surface temperature (SST) cooling^{5,6}, which is underpinned by the large impacts of Interdecadal Pacific Oscillation (IPO) on the GST^{16,17}. The IPO's impacts are similar but not identical to those exerted by El Niño¹⁸.

Consistent with previous findings^{5,6}, SST warming (cooling) occurs in the tropical Pacific during the acceleration (slowdown) periods (Supplementary Fig. 2). The SST change differences between the slowdown and acceleration periods bear a close resemblance to the pattern of the cold phase of the IPO¹⁹ or a La Niña-like decadal/multi-decadal variability²⁰. This indicates the possible importance of internal climate variability in modulating GW^{5,16}. However, notable differences in global SST changes exist among the acceleration and slowdown periods (Fig. 2). While the SST shows a similar warming in the tropical Pacific between the two acceleration periods (Fig. 2a,c), the equatorial central-eastern Pacific cooling during 2001–2012 is far stronger than that during 1940–1976 (Fig. 2b,d). Its magnitude is also greater than those

¹State Key Laboratory of Numerical Modeling for Atmospheric Sciences and Geophysical Fluid Dynamics, Institute of Atmospheric Physics, Chinese Academy of Sciences, Beijing 100029, China. ²University of Chinese Academy of Sciences, Beijing 100049, China. ³Australian Bureau of Meteorology, Melbourne, Victoria 3008, Australia. ⁴Laboratory for Regional Oceanography and Numerical Modeling, Qingdao National Laboratory for Marine Science and Technology, Qingdao 266237, China. ⁵Center for Monsoon System Research, Institute of Atmospheric Physics, Chinese Academy of Sciences, Beijing 100029, China. *e-mail: J.Luo@bom.gov.au; hg@mail.iap.ac.cn

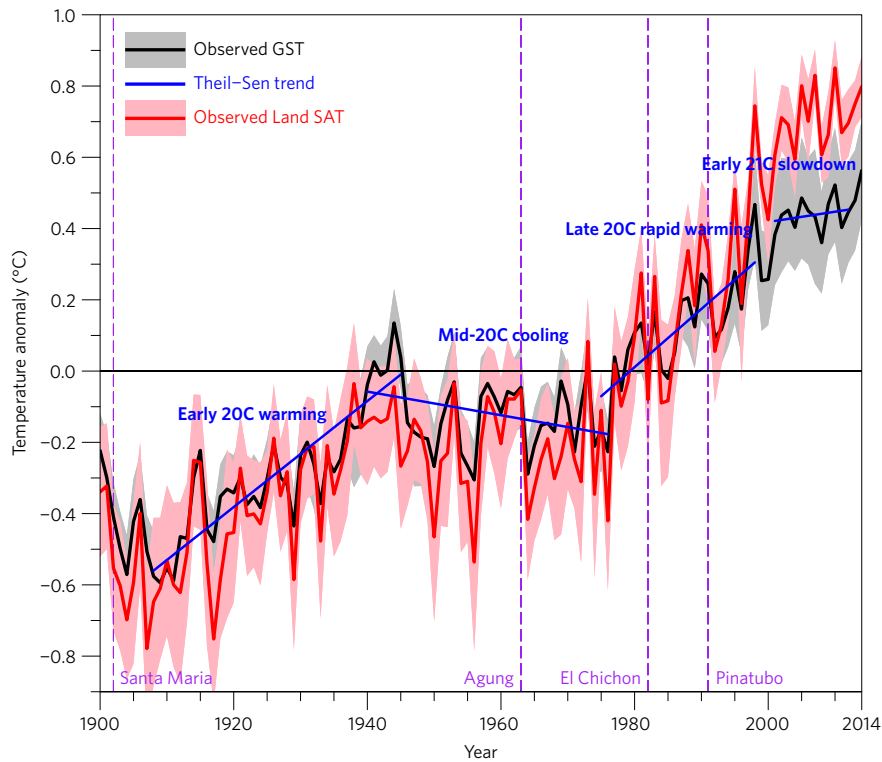


Figure 1 | Observed annual-mean globally averaged surface temperature (GST) and land surface air temperature (SAT) anomalies. Anomalies are relative to 1961–1990 climatology. The grey-shaded and pink-shaded areas represent one standard deviation of the differences among the observed GST and SAT, respectively. The solid blue lines indicate the Theil–Sen trend estimates for the early twentieth-century warming period (1908–1945), the mid-twentieth-century cooling period (1940–1976), the late twentieth-century rapid warming period (1975–1998) and the early twenty-first-century slowdown period (2001–2012), respectively. The vertical purple lines indicate the dates of major volcanic eruptions.

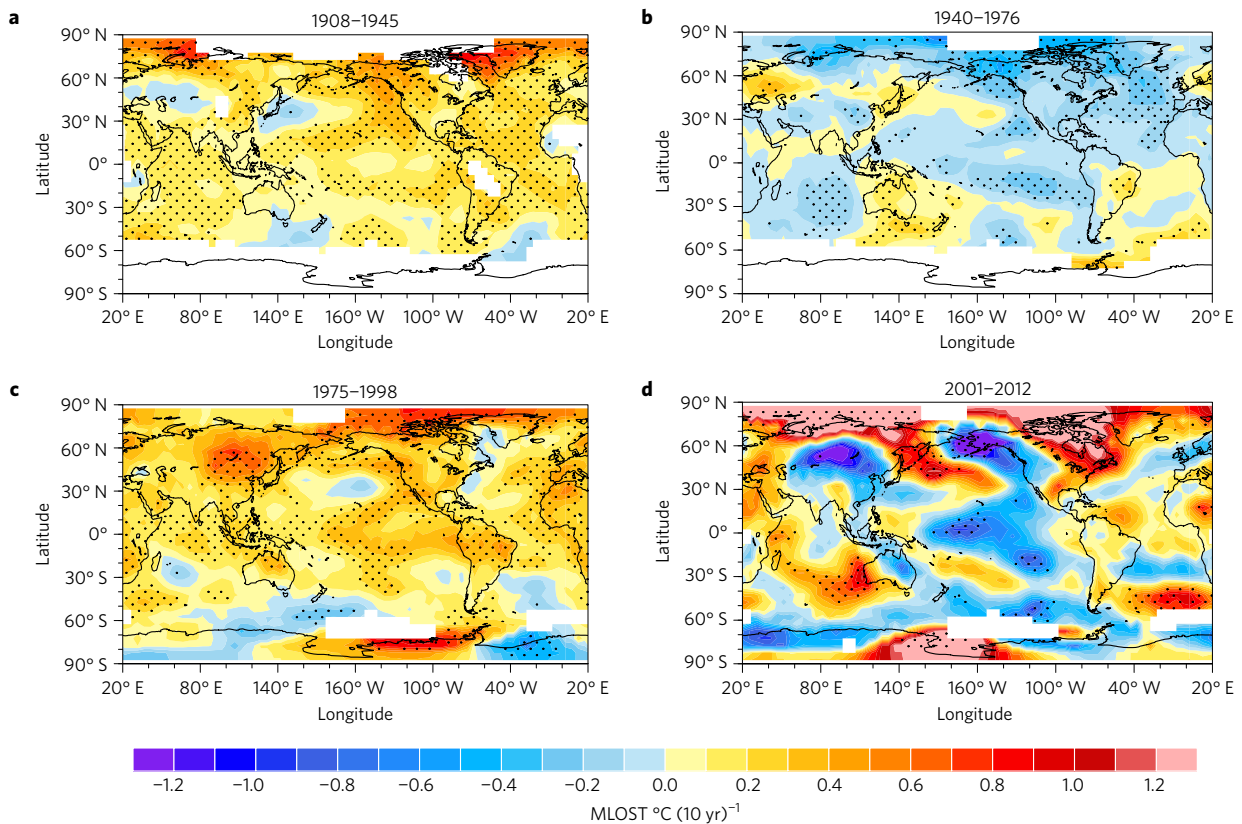


Figure 2 | Observed annual-mean merged land air temperature and ocean surface temperature (MLOST) trend patterns during the two acceleration and slowdown periods. a, 1908–1945. b, 1940–1976. c, 1975–1998. d, 2001–2012. The MLOST trends are estimated on the basis of the ensemble mean of four observations (Methods). White areas represent missing values. Stippling denotes 5% significance according to a two-sided Student’s *t*-test.

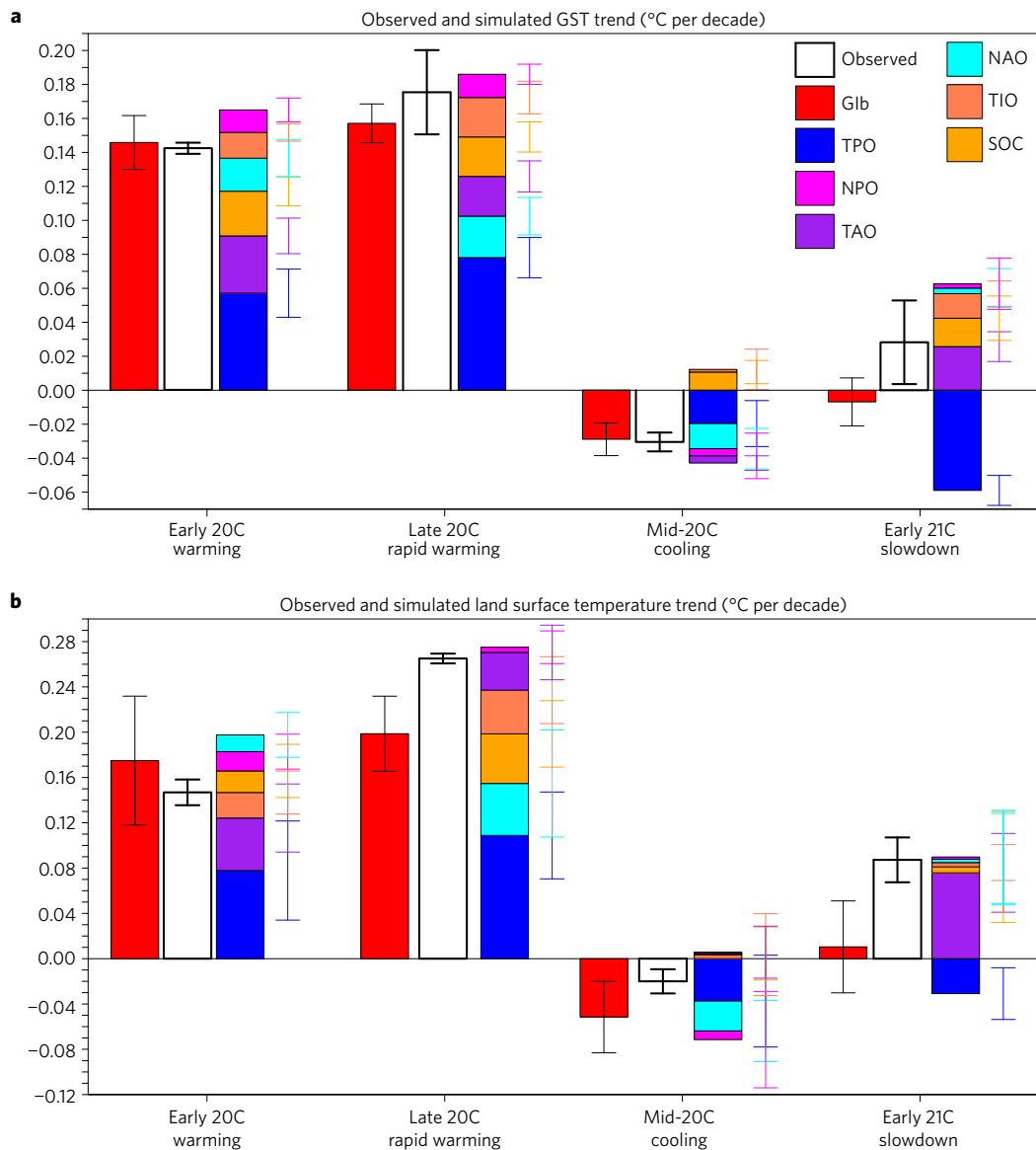


Figure 3 | Near-surface temperature trends during the two acceleration and two slowdown periods. a, Observed GST trends and simulated globally averaged near-surface air temperature trends. **b**, Observed and simulated land surface air temperature trends. The black empty bars indicate the observed ensemble mean GST and land surface air temperature of the four different data sources during each period. The simulated global near-surface air temperature trends include those forced by the global ocean (Glb), tropical Pacific Ocean (TPO), North Pacific Ocean (NPO), tropical Atlantic Ocean (TAO), North Atlantic Ocean (NAO), tropical Indian Ocean (TIO), and Southern Ocean (SOC). The model's simulations are based on six-member ensemble mean for each experiment (Methods). The order of the colour filled bars follows the order of the magnitudes of individual oceans' contributions. The error bars denote one standard deviation of the differences among the four observations (thick black bars) and across six members of each experiment (thin black bars for the global ocean forcing; and individual ocean forcings in colours indicated).

during the two acceleration periods. This is strongly at odds with the differences in GW rates between the slowdown and acceleration periods (compare Fig. 2 and Supplementary Table 1), although the amplified polar surface air temperature warming in the early twenty-first century (Fig. 2d) may partly offset the tropical Pacific-induced cooling effects²¹.

A prominent feature during the two acceleration periods is that significant SST warming appears across almost the entire global ocean except patches of weak cooling in the extratropics (Fig. 2). Consistently, surface air temperature warming occurs over the majority parts of global continents (Fig. 2a,c). In contrast, SST cooling during the two slowdown periods does not extend to the entire global ocean (Fig. 2b,d). In particular, extensive warming appeared in the Atlantic, the Indian Ocean, and the extratropical

Pacific during 2001–2012, opposite to the strong tropical Pacific cooling (Fig. 2d). Correspondingly, only limited areas of the global continents experienced significant cooling or warming during 2001–2012 (Fig. 2d). These results suggest that, while the tropical Pacific warming/cooling plays a major role, the SST changes in other basins may also have important influences on the GW rates^{22–24}.

As an attempt to quantify the relative contributions of individual ocean SST changes to the GW rates, we perform a set of atmospheric general circulation model experiments (Methods) in which the global SST trend during the two acceleration and slowdown periods is split into six regions, including the three tropical oceans that have predominant influences on the GST, and the North Atlantic, North Pacific and Southern Ocean (Supplementary Fig. 3). The simulations with the entire global SST trend forcing reproduce the

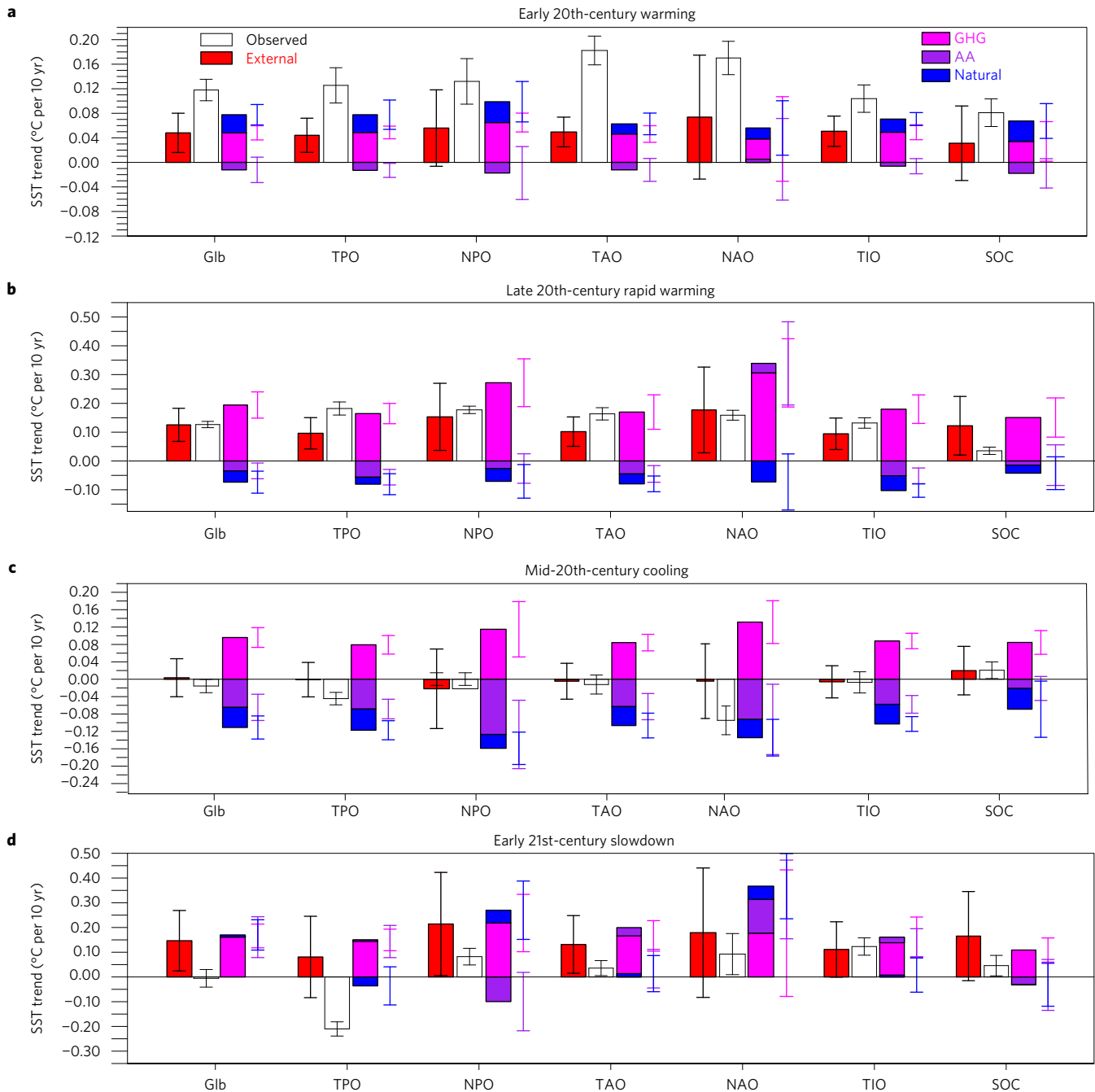


Figure 4 | Observed and CMIP5-simulated SST trends in the global ocean and six individual ocean basins. a–d, SST trends in the global ocean (Glb), tropical Pacific Ocean (TPO), North Pacific Ocean (NPO), tropical Atlantic Ocean (TAO), North Atlantic Ocean (NAO), tropical Indian Ocean (TIO) and Southern Ocean (SOC) from the observations, CMIP5 multi-model ensemble mean historical simulations (External, ideally represent the externally forced trends), multi-model ensemble mean simulation with greenhouse gas forcing only (GHG, Supplementary Table 2), with anthropogenic aerosol forcing only (AA), and with natural forcing only (Natural) for the early twentieth-century warming period (a), the late twentieth-century rapid warming period (b), the mid-twentieth-century cooling period (c) and the early twenty-first-century slowdown period (d). The error bars indicate one standard deviation of the differences among four observations (thick black bars) and across CMIP5 models (thin black bars for historical simulations; and individual radiative forcings in colours indicated).

observed GST and land SAT warming during the early and late twentieth century fairly well (Fig. 3a,b, red filled and black empty bars). The model also successfully reproduces the observed GST and land SAT cooling in the mid-twentieth century (Fig. 3a,b). The recent slowdown, however, is not well simulated. While the observations show a muted warming, the model produces a weak GST cooling and a weak land SAT warming; this may be partly because Arctic amplification²¹ is not captured (Supplementary Fig. 4d) due to the

fact that observed sea-ice changes are not prescribed in the model. Besides, model’s GHGs concentrations are fixed for each period and therefore the large direct forcing effect is not simulated (Methods).

The simulated land SAT trends are weaker than the observed (Supplementary Fig. 4c,d), particularly for the late twentieth-century rapid warming and recent slowdown periods; this suggests a role of direct external forcing²⁵ (Supplementary Information and Supplementary Table 3). The estimated direct forcing effect has

persistently increased since 1900, in accordance with the increased trend of CO₂. Despite model deficiencies (Supplementary Information) and possible impacts of internal variability^{26,27}, the spatial distributions of observed GW trends during the two acceleration and slowdown periods (compare Fig. 2 and Supplementary Fig. 4) are generally well reproduced by the model with the global SST trend forcing, with pattern correlation reaching approximately 0.74, 0.82, 0.57 and 0.46, respectively.

The summed contributions of the SST changes in the six basins to the GW rates during the four inter-decadal periods are close (albeit not equal) to those simulated with the global SST trend forcing (Fig. 3, see Supplementary Information for the nonlinear effect discussion). During the two accelerated warming periods in the early and late twentieth century, the tropical Pacific (occupying ~21.1% of global area) SST warming plays the largest role, accounting for approximately 34% (39%) and 42% (39%) of the total GST (land SAT) warming rates, respectively (Fig. 3a,b). In the early twentieth century, the tropical Atlantic (~8.5% of global area) SST warming plays the second largest role (explaining ~20% and ~23% of the total GST and land SAT warming rates, respectively). In addition, for the two accelerated warming periods, the total SST warming in the Southern Ocean (~22.5% of global surface), North Atlantic (~4.1% of global area), tropical Indian Ocean (~8.4% of global area) and North Pacific (~5.8% of global area) accounts for nearly half and ~45% of the summed GST rates, respectively. These four oceans also explain large portions of land SAT warming rates (totally ~38% and ~49% during the two accelerated warming periods, respectively) and produce extensive warming over the global lands (Supplementary Fig. 5 and Supplementary Information).

During the mid-twentieth century, the cooling in the tropical Pacific plays an important role in the GST cooling, which is nearly equal to the summed contributions of the SST cooling in the North Atlantic, tropical Atlantic and North Pacific (Fig. 3a). Similarly, the summed contribution of the North Atlantic and North Pacific SST cooling to the global land SAT cooling is as important as that of the tropical Pacific (Fig. 3b). In contrast, the SST warming in the Southern Ocean and tropical Indian Ocean acts to increase the GST and land SAT by ~30% and ~7%, respectively, which tends to partly offset the cooling effects of the other oceans (Supplementary Fig. 6 and Supplementary Information). The compensation effect among the different oceans is more striking during the recent slowdown period. The strong cooling in the tropical Pacific generates a GST (land SAT) cooling of approximately -0.059 °C (-0.031 °C) per decade, consistent with the previous finding^{5,6}. However, the induced GST and land SAT cooling is completely offset or overwhelmed by the summed warming effects of the tropical Atlantic and Indian Ocean, Southern Ocean, North Pacific and North Atlantic (Fig. 3 and Supplementary Fig. 7 and Supplementary Information).

In summary, our results reveal distinct impacts of individual basin's SST changes on the GW rates between the acceleration and slowdown periods. In the acceleration cases, the SST warming in all the oceans acts jointly to generate strong GW rates. In contrast, in the slowdown cases, the GST cooling induced by the tropical Pacific cooling is reduced or negated by the warming effects in the other oceans, leading to weak GW rates.

Thus, it is the SST changes in multiple oceans, not merely those in the tropical Pacific, that are crucial to determine the GW rates. On the basis of the Coupled Model Intercomparison Project Phase 5 (CMIP5) simulations with various radiative forcing (Methods), we explore possible causes of observed SST changes in individual oceans during the acceleration and slowdown periods. The observed SST warming in the global ocean and individual basins in the early twentieth century is partly reproduced by the multi-model historical simulations due to increased GHGs and natural forcing (Fig. 4a). Note that the difference between the observed and model

simulations could be caused by internal variability²⁸ and errors in models²⁹ and historical forcings. In contrast, the late twentieth-century SST warming in the global ocean and most of the individual oceans is largely simulated in response to increased GHGs (Fig. 4b), which is partly offset by the cooling effects of anthropogenic aerosols and natural forcing.

In agreement with previous studies³⁰, our results suggest that increased anthropogenic aerosols during the mid-twentieth-century cooling period induce large cooling in global ocean and individual oceans, which overwhelms the warming effects of increased GHGs (Fig. 4c). However, large discrepancy is seen between the observed and multi-model historical simulations in the tropical Pacific and North Atlantic, which bears a resemblance to the observed SST trend pattern in the mid-twentieth century (Supplementary Fig. 8e). The discrepancy between the observations and multi-model historical simulations becomes more apparent in the tropical Pacific during the recent slowdown period (Fig. 4d and Supplementary Fig. 8g), suggesting that internal variability and/or model errors²⁹ may play an important role. The external radiative forcing produces generally uniform warming across the global ocean, largely accounting for the basin-wide average SST warming in the other oceans (Fig. 4d and Supplementary Fig. 8h).

The results imply that the SST changes in global and regional oceans during the two accelerations and slowdowns are driven by complicated and distinct mechanisms, which cannot be solely explained by modelled response to external radiative forcing. Improved understanding and projection of the distinct SST changes in multiple oceans between the multi-decadal GW acceleration and slowdown periods could help achieve a more accurate estimate of the future GW rate to better meet the GW target of the Paris Conference, compared with that based on increasing GHG emissions alone and/or a single-ocean SST change alone.

Methods

Methods, including statements of data availability and any associated accession codes and references, are available in the [online version of this paper](#).

Received 12 September 2016; accepted 27 April 2017; published online 12 June 2017

References

- Kosaka, Y. & Xie, S.-P. The tropical Pacific as a key pacemaker of the variable rates of global warming. *Nat. Geosci.* **9**, 669–673 (2016).
- Meehl, G. A., Hu, A., Santer, B. D. & Xie, S.-P. Contribution of the Interdecadal Pacific Oscillation to twentieth-century global surface temperature trends. *Nat. Clim. Change* **6**, 1005–1008 (2016).
- Knutson, T. R., Zhang, R. & Horowitz, L. W. Prospects for a prolonged slowdown in global warming in the early 21st century. *Nat. Commun.* **7**, 13676 (2016).
- IPCC: Summary for Policymakers. In *Climate Change 2013: The Physical Science Basis* (eds Stocker, T. F. et al.) (Cambridge Univ. Press, 2013).
- Meehl, G. A., Arblaster, J. M., Fasullo, J. T., Hu, A. & Trenberth, K. E. Model-based evidence of deep-ocean heat uptake during surface-temperature hiatus periods. *Nat. Clim. Change* **1**, 360–364 (2011).
- Kosaka, Y. & Xie, S.-P. Recent global-warming hiatus tied to equatorial Pacific surface cooling. *Nature* **501**, 403–407 (2013).
- Clement, A. & DiNezio, P. The tropical Pacific ocean—back in the driver's seat? *Science* **343**, 976–978 (2014).
- Fyfe, J. C. et al. Making sense of the early-2000s warming slowdown. *Nat. Clim. Change* **6**, 224–228 (2016).
- Hulme, M. 1.5 °C and climate research after the Paris Agreement. *Nat. Clim. Change* **6**, 222–224 (2016).
- Hartmann, D. et al. in *Climate Change 2013: The Physical Science Basis* (eds Stocker, T. F. et al.) 159–254 (IPCC, Cambridge Univ. Press, 2013).
- Dai, A., Fyfe, J. C., Xie, S.-P. & Dai, X. Decadal modulation of global surface temperature by internal climate variability. *Nat. Clim. Change* **5**, 555–559 (2015).
- Watanabe, M. et al. Contribution of natural decadal variability to global warming acceleration and hiatus. *Nat. Clim. Change* **4**, 893–897 (2014).

13. Santer, B. *et al.* Separating signal and noise in atmospheric temperature changes: the importance of timescale. *J. Geophys. Res.* **116**, D22105 (2011).
14. Karl, T. R. *et al.* Possible artifacts of data biases in the recent global surface warming hiatus. *Science* **348**, 1469–1472 (2015).
15. Bindoff, N. L. *et al.* in *Climate Change 2013: The Physical Science Basis* (eds Stocker, T. F. *et al.*) 867–952 (IPCC, Cambridge Univ. Press, 2013).
16. Meehl, G. A., Hu, A., Arblaster, J. M., Fasullo, J. & Trenberth, K. E. Externally forced and internally generated decadal climate variability associated with the interdecadal Pacific oscillation. *J. Clim.* **26**, 7298–7310 (2013).
17. Trenberth, K. E., Fasullo, J. T., Branstator, G. & Phillips, A. S. Seasonal aspects of the recent pause in surface warming. *Nat. Clim. Change* **4**, 911–916 (2014).
18. Pan, Y. H. & Oort, A. H. Global climate variations connected with sea surface temperature anomalies in the eastern equatorial Pacific Ocean for the 1958–73 period. *Mon. Weath. Rev.* **111**, 1244–1258 (1983).
19. Power, S., Casey, T., Folland, C., Colman, A. & Mehta, V. Inter-decadal modulation of the impact of ENSO on Australia. *Clim. Dynam.* **15**, 319–324 (1999).
20. Luo, J.-J. & Yamagata, T. Long-term El Niño–Southern Oscillation (ENSO)-like variation with special emphasis on the South Pacific. *J. Geophys. Res.* **106**, 22211–22227 (2001).
21. Cowtan, K. & Way, R. G. Coverage bias in the HadCRUT4 temperature series and its impact on recent temperature trends. *Q. J. R. Meteorol. Soc.* **140**, 1935–1944 (2014).
22. Chen, X. & Tung, K.-K. Varying planetary heat sink led to global-warming slowdown and acceleration. *Science* **345**, 897–903 (2014).
23. Drijfhout, S. *et al.* Surface warming hiatus caused by increased heat uptake across multiple ocean basins. *Geophys. Res. Lett.* **41**, 7868–7874 (2014).
24. Keenlyside, N. S. & Ba, J. Prospects for decadal climate prediction. *WIREs Clim. Change* **1**, 627–635 (2010).
25. Booth, B. B., Dunstone, N. J., Halloran, P. R., Andrews, T. & Bellouin, N. Aerosols implicated as a prime driver of twentieth-century North Atlantic climate variability. *Nature* **484**, 228–232 (2012).
26. Swart, N. C., Fyfe, J. C., Hawkins, E., Kay, J. E. & Jahn, A. Influence of internal variability on Arctic sea-ice trends. *Nat. Clim. Change* **5**, 86–89 (2015).
27. Screen, J. A. & Francis, J. A. Contribution of sea-ice loss to Arctic amplification is regulated by Pacific Ocean decadal variability. *Nat. Clim. Change* **6**, 856–860 (2016).
28. Tett, S. F. *et al.* Estimation of natural and anthropogenic contributions to twentieth century temperature change. *J. Geophys. Res.* <http://doi.org/10.1029/2000JD000028> (2002).
29. Luo, J.-J., Wang, G. & Dommenges, D. May common model biases reduce CMIP5's ability to simulate the recent Pacific La Niña-like cooling? *Clim. Dynam.* <http://dx.doi.org/10.1007/s00382-017-3688-8> (2017).
30. Wilcox, L. J., Highwood, E. J. & Dunstone, N. J. The influence of anthropogenic aerosol on multi-decadal variations of historical global climate. *Environ. Res. Lett.* **8**, 024033 (2013).

Acknowledgements

This work was supported by the National Natural Science Foundation of China (41425019 and 41661144016), and the Public Science and Technology Research Funds Projects of Ocean (201505013). P.W. was supported by the National Natural Science Foundation of China (41375112). We thank the Max Plank Institute for Meteorology for providing the ECHAM5 atmospheric general circulation model, the World Climate Research Programme's Working Group on Coupled Modeling for providing the CMIP multi-model data sets, S.-P. Xie, C. Chung and P. Reid for their helpful comments and/or discussions.

Author contributions

S.-L.Y., J.-J.L. and G.H. conceived the research; J.-J.L. and S.-L.Y. designed the model experiments; S.-L.Y. and P.W. performed numerical simulations; S.-L.Y. performed the data analysis; J.-J.L. and S.-L.Y. wrote the paper; J.-J.L. and G.H. supervised this study.

Additional information

Supplementary information is available in the [online version of the paper](#). Reprints and permissions information is available online at www.nature.com/reprints. Publisher's note: Springer Nature remains neutral with regard to jurisdictional claims in published maps and institutional affiliations. Correspondence and requests for materials should be addressed to J.-J.L. or G.H.

Competing financial interests

The authors declare no competing financial interests.

Methods

Data sets. We use the Hadley Centre-Climate Research Unit merged land air temperature and ocean surface temperature (MLOST) version 4.4.0.0 median (HadCRUT4)³¹ and global land near-surface air temperature (SAT) version 4.4.0.0 (CRUTEM4)³², the National Aeronautics and Space Administration Goddard Institute for Space Studies (NASA GISS) GISTEMP³³ with 1,200 km smoothing and global mean land SAT, the National Oceanic and Atmospheric Administration National Climatic Data Center (NOAA NCDC) MLOST version 4.0.0 (ref. 34) and the Global Historical Climatology Network land SAT version 3.3.0, the International Surface Temperature Initiative (ISTI) databank¹⁴ MLOST time series and gridded data sets and land SAT time series for the period 1900–2014. We use monthly mean Centennial In Situ Observation-Based Estimates of the Variability of Sea Surface Temperature (COBE-SST) and version 2 (COBE-SST2)³⁵, corrected Extended Reconstructed Sea Surface Temperature version 4 (ERSST v4)¹⁴, and merged Hadley-Optimal-Interpolation sea surface temperature and sea-ice concentration data sets³⁶ for the period 1900–2012. To reduce observational uncertainty, the ensemble mean of the observed MLOST, land SAT and SST from the four different data sets is employed in this study.

We also analyse the multi-model ensemble mean SST provided by the Coupled Model Intercomparison Project³⁷ (CMIP5) of the Intergovernmental Panel on Climate Change. 128 members of 42 models' historical simulations that are extended from 2006 to 2012 on the basis of RCP4.5 scenario runs, 35 members of 9 models' greenhouse gas (GHG) forcing simulations, 38 members of 10 models' natural forcing simulations, and 21 members of 5 models' anthropogenic aerosol forcing simulations for the period 1900–2012 (Supplementary Table 2) are analysed to investigate causes of the observed SST changes in multiple ocean basins (Fig. 4 and Supplementary Fig. 8). To reduce model uncertainty, we calculate the multi-model ensemble mean of each scenario experiment using the same weight for each model.

Analysis methods. We adopt an optimal piecewise linear regression to fit the trends with increasing time intervals of observed GST and MLOST. On the basis of the following three thresholds: a maximum magnitude of GST trends above 95% confidence level, relatively low observational uncertainty, and a high percentage of grid boxes that show statistical significant trends above 95% confidence level, we detect two robust accelerated warming periods in the early twentieth century (1908–1945) and the late twentieth century (1975–1998), and two global warming (GW) slowdown periods in the mid-twentieth century (1940–1976) and the early twenty-first century (2001–2012) (Supplementary Fig. 1). Note that some of the time windows are slightly overlapped, representing an uncertainty in defining the periods of GW accelerations and slowdowns. Removing the overlapped time intervals among these periods gives similar results. The least-square linear regression and Theil–Sen slope³⁸ methods are used to estimate the observed GST trends, with the statistical significance being performed with the Student's *t*-test and Mann–Kendall test (Supplementary Table 1). The observed SST and MLOST trends are computed at each grid box where the data availability covers more than 80% of the years during individual GW acceleration and slowdown periods.

AGCM sensitivity experiments. The Max Planck Institute for Meteorology atmospheric general circulation model³⁹ (AGCM, ECHAM5.4.1) is used to examine the response of globally averaged surface temperature (GST) to the observed SST trend forcing in the global ocean and individual oceans. Given the important impacts of the tropical SST on the GST, we first split the tropical oceans into the tropical Pacific Ocean (TPO), tropical Atlantic Ocean (TAO), and tropical Indian Ocean (TIO). The extratropical regions are then separated into the North Pacific Ocean (NPO), North Atlantic Ocean (NAO) and Southern Ocean (SOC) (Supplementary Fig. 3). We adopt ECHAM5 T63L31, which has a horizontal resolution of ~209 km and 31 vertical layers³⁹. In the model sensitivity runs, we prescribe the observed SST trends in the global ocean and six different basins separately with carbon dioxide (CO₂) concentration being fixed to the level at the centre year of the period during 1908–1945, 1975–1998, 1940–1976 and

2001–2012, respectively. An additional model sensitivity experiment, in which the observed CO₂ trend during 1958–2012 is prescribed but the global SST forcing is fixed with the climatological monthly mean of 1981–2010, produces a GW rate of ~0.028 °C per decade and a land SAT warming rate of ~0.07 °C per decade that accounts for ~22% and ~32% of the observed GW rate of ~0.13 °C per decade and observed land SAT warming rate of ~0.22 °C per decade averaged during 1958–2012, respectively. To avoid potential instability, a linear buffer zone with a width of five latitudes and longitudes is applied to prescribe the observed SST trends in individual basins (for example, in the tropical Pacific Ocean, the linear buffer zone extends from 30° N to 35° N, 35° S to 30° S, and 115° E to 120° E). For each of the model experiments that are integrated for 30 model years, we perform six-member ensemble simulations in which the same SST and CO₂ forcing is prescribed but their initial conditions are different and provided by an additional model run with climatological SST forcing. Results shown are based on the six-member ensemble mean of individual model experiments. Note that the global mean results are similar if model outputs in areas where the observations are missing during the GW acceleration and slowdown periods are excluded in the model's calculations.

Data availability. The data that support the findings of this study are available from the corresponding authors on request. The model outputs from the ECHAM5 sensitivity experiments are available to readers on request. Other model data are available from the CMIP5 data portal (http://cmip-pcmdi.llnl.gov/cmip5/data_portal.html). Sources for the observed data sets are: HadCRUT4 (ref. 31) and CRUTEM4 (ref. 32) (accessed on 1 October 2015): <http://www.metoffice.gov.uk/hadobs/index.html>; GISTEMP³³ (accessed on 1 October 2015): <https://data.giss.nasa.gov/gistemp/>; NOAA NCDC³⁴ (accessed on 30 August 2015): <https://www.ncdc.noaa.gov/data-access/marineocean-data/mlost>; ISTI¹⁴ (accessed on 15 July 2015): <http://www.surface-temperatures.org>; COBE-SST and COBE-SST2 (ref. 35) (accessed on 10 August 2015): <https://climatedataguide.ucar.edu/climate-data/sst-data-cobe-centennial-situ-observation-based-estimates>; ERSST v4 (ref. 14) (accessed on 10 August 2015): <https://www.ncdc.noaa.gov/data-access/marineocean-data/extended-reconstructed-sea-surface-temperature-ersst-v4>; Hurrell SST³⁶ (accessed on 15 August 2015): <https://cdp.ucar.edu/security/loginout.htm>.

References

- Morice, C. P., Kennedy, J. J., Rayner, N. A. & Jones, P. D. Quantifying uncertainties in global and regional temperature change using an ensemble of observational estimates: the HadCRUT4 data set. *J. Geophys. Res.* **117**, D08101 (2012).
- Jones, P. *et al.* Hemispheric and large-scale land-surface air temperature variations: an extensive revision and an update to 2010. *J. Geophys. Res.* **117**, D05127 (2012).
- Hansen, J., Ruedy, R., Sato, M. & Lo, K. Global surface temperature change. *Rev. Geophys.* **48**, RG4004 (2010).
- Vose, R. S. *et al.* NOAA's merged land-ocean surface temperature analysis. *Bull. Am. Meteorol. Soc.* **93**, 1677–1685 (2012).
- Hirahara, S., Ishii, M. & Fukuda, Y. Centennial-scale sea surface temperature analysis and its uncertainty. *J. Clim.* **27**, 57–75 (2014).
- Hurrell, J. W., Hack, J. J., Shea, D., Caron, J. M. & Rosinski, J. A new sea surface temperature and sea ice boundary dataset for the Community Atmosphere Model. *J. Clim.* **21**, 5145–5153 (2008).
- Taylor, K. E., Stouffer, R. J. & Meehl, G. A. An overview of CMIP5 and the experiment design. *Bull. Am. Meteorol. Soc.* **93**, 485–498 (2012).
- Sen, P. K. Estimates of the regression coefficient based on Kendall's tau. *J. Am. Stat. Assoc.* **63**, 1379–1389 (1968).
- Roegner, E. *et al.* *The atmospheric general circulation model ECHAM 5. PART I: model description* Report 349 (Max-Planck-Institut für Meteorologie, 2003).